Flows in parallelepiped cells of nematic liquid crystals

Ervanggis Minggar Kusumasari,[1] Suharli AJ,[1] Bhisma Mahendra,[2] and Yusril Yusuf[1,*]
[1]*Department of Physics, Faculty of Mathematics and Natural Sciences, Universitas Gadjah Mada, Sekip Utara, Yogyakarta 55281, Indonesia*
[2]*Faculty of Engineering, Universitas Singaperbangsa Karawang, Karawang, West Java 41361, Indonesia*

(Received 10 August 2022; accepted 5 December 2022; published 22 December 2022)

We identified three types of flow in a nematic liquid crystal parallelepiped cell subjected to an ac electric field at low frequency. Our observations show the existence of translational flow, backflow, and convection flow in parallelepiped cells. We measured the backflow velocity by introducing microparticles into the sample. The backflow velocity at the normalized voltage $\varepsilon = 0.05$ is approximately 0.1 μm/s. It has the same order as the translational flow velocity at $\varepsilon = 0.05$. Furthermore, convection flow occurs earlier than translational flow.

DOI: 10.1103/PhysRevE.106.064702

I. INTRODUCTION

The effect of an electric field applied to a nematic liquid crystal (NLC) has attracted increasing attention [1–6]. It has been studied specifically in electrohydrodynamic (EHD) instability to understand pattern formation in materials with anisotropic properties [7–11]. One of the most popular patterns is the Williams domain (WD) [1], the stationary bright and dark pattern that appears when an NLC is given an electric field at a certain voltage. WD formation can be explained by the Carr-Helfrich mechanism [4,5,12]. In principle, the Coulomb force resulting from the interaction of the electric field and the fluctuation of the director will overcome the viscoelastic force at the critical voltage (V_C), resulting in EHD instability [13,14]. EHD instability has two different frequency regimes [13], separated by a *cutoff* frequency (f_C). These are low-frequency (conduction) ($f < f_C$) and high-frequency (dielectric) ($f > f_C$) regimes [13]. In the conduction regime, normal or oblique rolls with the wavelength λ, of the order of the sample thickness d, are observed (e.g., WD pattern). In the dielectric regime, the dielectric roll pattern ($\lambda \ll d$) is observed.

Studies [15,16] observed that the WD pattern is not static but moves slowly. This pattern is known as traveling waves (TWs) [15–19]. The mechanism of this pattern is explained by the weak-electrolyte model (WEM) [20–23]. The WEM mechanism incorporates the dissociation-recombination reaction of an ionic dopant and its effect on conductivity [24,25]. In WEM, the electric current is assumed to be carried by positive and negative ionic charge carriers with constant mobility coupled with a dissociation-recombination reaction. The conductivity, which is proportional to the sum of the densities of the two ions as measured by the mobility, becomes a new dynamic variable (charge carrier model) [22]. The local deviation of the coupled conductivity with the director field will stabilize the main destabilizing effect in the Carr-Helfrich model. The competition between the two effects, which cancel each other out, will result in oscillating convection (TWs) [20]. The observation of TWs requires a huge generator voltage; for example, the value of $V_C = 47.8\ V$ ($f = 600$ Hz) [16].

A TW-like pattern at low frequency can be observed by cell modification [26]. Planar cells are modified by adding a nonconvective site and are called parallelepiped cells. The cells have a horizontal electric field component due to the parallelepiped cell geometry. Ion accumulation occurs in the nonconvective part of the cell so that the conductivity perpendicular to the electric field is no longer homogeneous, and the WEM mechanism applies. The observed pattern is a WD pattern that moves slowly like a TW pattern. This pattern is known as translational flow. However, the translational flow has different characteristics from the TW pattern. The TW pattern moves randomly parallel to the director, whereas the translational flow moves uniformly from the edges to the center of the cell. The pattern velocity of translational flow decreases as the applied voltage and frequency increase, whereas the TW pattern is the opposite. However, the research [26] raises questions regarding backflow, how mass flow occurs in translational flow, and how flow occurs under threshold voltage. In this study, we focused on investigating the backflow and mass flow of NLCs related to translational flow to complement the information from the previous study [26]. In addition, we investigated the presence or absence of flow below the threshold voltage and in the nonconvection part of the cell. For this reason, in this study, we used microparticles that were inserted into the sample.

II. EXPERIMENT

We used 2 cm × 2.5 cm indium tin oxide glass. The glass was then etched, and the area to be exposed to the electric field was 1 cm × 1 cm. Two pieces of glass were then coated with polyvinyl alcohol and rubbed. We made planar [27–29] cells using two glasses arranged in parallel and separated by two Mylar spacers with a thickness of 50 μm. We made an indented area of planar sandwich cells (Δl) [Fig. 5]. This sample was named parallelepiped cells [26] and divided into seven segments on the x axis as described in Fig. 5. The length of each segment is 1200 μm. In this study, our observations were

*yusril@ugm.ac.id

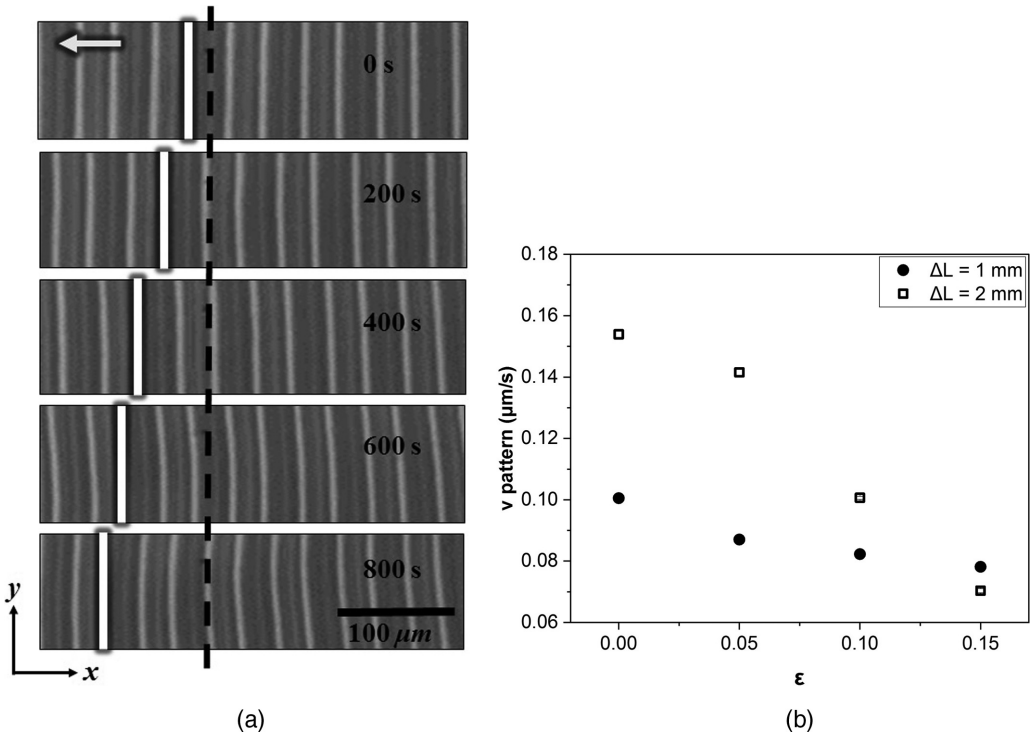

FIG. 1. (a) The pattern motion (translational flow) in a parallelepiped cell on $X = 7$ (the right end of the cell) with $\Delta l = 1$ mm at $f = 100$ Hz and $\varepsilon = 0.10$. The black dashed line is the reference point. The white lines and arrows indicate the movement of the pattern. (b) Dependence of pattern velocity (v_p) on ε.

made on segment $X = 7$ (the right end of the cell). We made samples with Δl of 1 and 2 mm. The cells were filled with 4-methoxybenzylidene-4-butylaniline (MBBA) NLCs doped with 0.02% tetra-*n*-butylammonium bromide (TBAB). To observe the flow, we added a small amount of microparticle (Micropearl, Sekisui Chemical Co., L.td.) 3.75 μm in diameter to the mixture of MBBA and TBAB. This method is quite adequate, as has been done in several studies [30–34].

Ac voltage was applied to samples using a function synthesizer (WF1974, NF Corporation) and an amplifier (F10AD, FLC Electronics). The voltage was varied in the form of normalized voltage $\varepsilon = (\frac{V}{V_c})^2 - 1$, where V_c is the threshold voltage for the WD pattern. The frequency was set at a value of 100 Hz. Observations were made by recording images for 60 min using a charge coupled device camera (KPF30PLC, Hitachi Ltd.) mounted on a microscope (CST-15, Carton Optical Industry, Ltd.). At each voltage variation, the sample was given a relaxation time of 10 min. The sample temperature was maintained at 30 °C using a controller (DB500, CHINO Works America, Inc.). All sample images were analyzed using IMAGE-J software to obtain information on pattern velocity (v_p), microparticle velocity (v_m), and backflow in translational flow.

III. RESULTS

We measured the pattern velocity on the segment of $X = 7$ (the right end of the cell) [Fig. 5]. Figure 1(a) shows the motion of the pattern with a normalized voltage of $\varepsilon = 0.10$ and a frequency of 100 Hz. The motion is shown by a white line that slowly moves to the left side against the reference (dashed black line). The pattern velocity was measured from a sample of $\Delta l = 1$ mm and $\Delta l = 2$ mm against ε. The results are shown in Fig. 1(b), which shows that the pattern velocity decreases with increasing voltage, as obtained in [26]. The pattern velocity at ε slightly above zero has the largest value, $(100.5 \pm 0.7) \times 10^{-3}$ μm/s for sample $\Delta l = 1$ mm and $(154 \pm 1) \times 10^{-3}$ μm/s for sample $\Delta l = 2$ mm. Overall, Fig. 1(b) shows that the pattern velocity at $\Delta l = 2$ mm is greater than that of the sample $\Delta l = 1$ mm. In this study, the variation of epsilon was limited to 0.15. This is because, at epsilon >0.15, the translational flow will be mixed with the movement of the fluctuating Williams domain. This occurs when a branching appears in the WD pattern, and the translational flow cannot be observed properly.

Figure 2(a) shows the oscillating motion of the microparticle (marked with a white circle). This motion can be seen from the reference point (dashed black line). First, at $t = 10$ s, the microparticle is near the dashed black line; then the microparticle moves slowly to the right until it reaches its maximum point at $t = 30$ s. At $t = 50$ s, the particle moves to the left until it arrives near its initial position. The microparticle appears to move in and out of focus. This result shows that the particle's orbit is circular [30], which indicates convection flow. Our experiments showed that the microparticles do not simply oscillate, but at a particular time, the microparticle shows a displacement from one roll to another roll. This result is discussed in Fig. 3.

Figure 2(b) shows the graph of the velocity of a microparticle (v_m) against ε. At a small value of ε, the microparticle velocity for sample $\Delta l = 1$ mm is almost the same as $\Delta l = 2$ mm. At large ε values, the

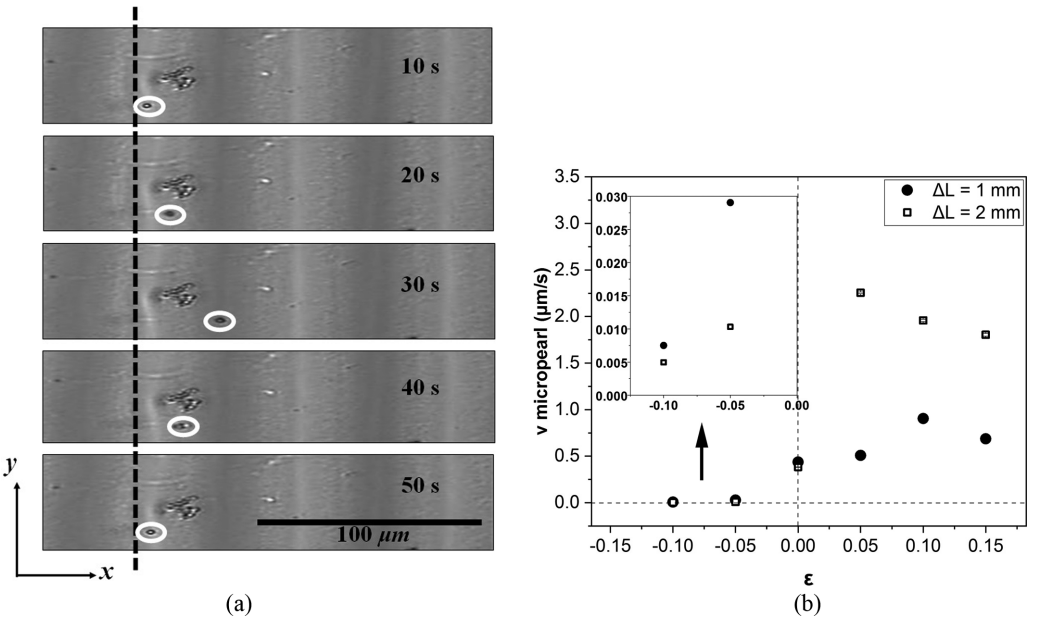

(a) (b)

FIG. 2. (a) The motion of a particle (microparticle) in a parallelepiped cell on $X = 7$ with $\Delta l = 1$ mm, $f = 100$ Hz and $\varepsilon = 0.10$. The black dashed line indicates the reference point, whereas the white circle represents particle motion. (b) Dependence of particle (microparticle) velocity (v_m) on ε.

microparticle velocity in the $\Delta l = 2$ mm sample is about two to three times the microparticle velocity in the $\Delta l = 1$ mm sample. For sample $\Delta l = 1$ mm, the microparticle velocity increased until the value of $\varepsilon = 0.10$, but decreased at $\varepsilon = 0.15$. For the sample $\Delta l = 2$ mm, microparticle velocity increased until the value of $\varepsilon = 0.05$ and decreased again at $\varepsilon = 0.10$. We also observed microparticle motion under threshold voltage ($\varepsilon < 0$). The microparticle slightly vibrates at speeds of 7.5×10^{-3} μm/s ($\Delta l = 1$ mm) and 4.9×10^{-3} μm/s ($\Delta l = 2$ mm) at $\varepsilon = -0.10$. The microparticle velocity at $\varepsilon = -0.05$ is 29×10^{-3} μm/s ($\Delta l = 1$ mm) and 10×10^{-3} μm/s ($\Delta l = 2$ mm). This can be explained as at $\varepsilon < 0$, convection flow begins to occur, even though the WD pattern has not been observed. This result indicates that convection flow occurs earlier than translational flow. At $\varepsilon > 0$, the microparticle velocity tends to increase because a perfect convection flow has formed, and the velocity increases coupled with the translational flow. In the sample $\Delta l = 2$ mm, the microparticle velocity reached its maximum value at $\varepsilon = 0.05$. This can be explained by the following. At this voltage value, the WD pattern is fully developed, and the convection flow has reached its maximum velocity, coupled with the presence of translational flow velocity. However, at $\varepsilon = 0.10$, the microparticle velocity tends to decrease again. This occurred because, at this voltage, the convection flow has reached a constant value, so the microparticle velocity

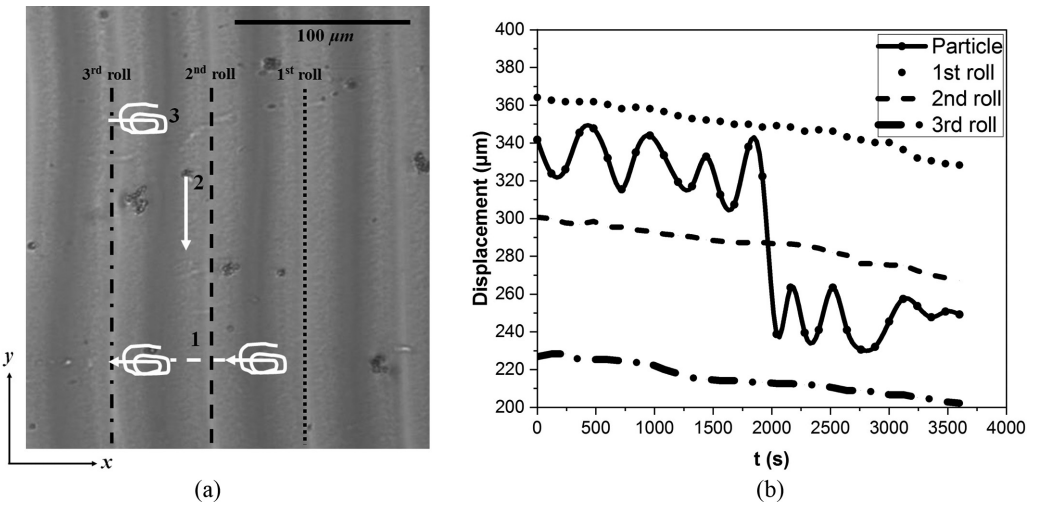

(a) (b)

FIG. 3. (a) The trajectory of the particle (microparticle) in a parallelepiped cell with $\Delta l = 1$ mm, $f = 100$ Hz, and $\varepsilon = 0.05$. (1) Translational flow starting with convection flow, (2) the effect of backflow, (3) convection flow. (b) The position of pattern and particle (microparticle) every 120 s ($\Delta l = 1$ mm, $f = 100$ Hz, and $\varepsilon = 0.05$).

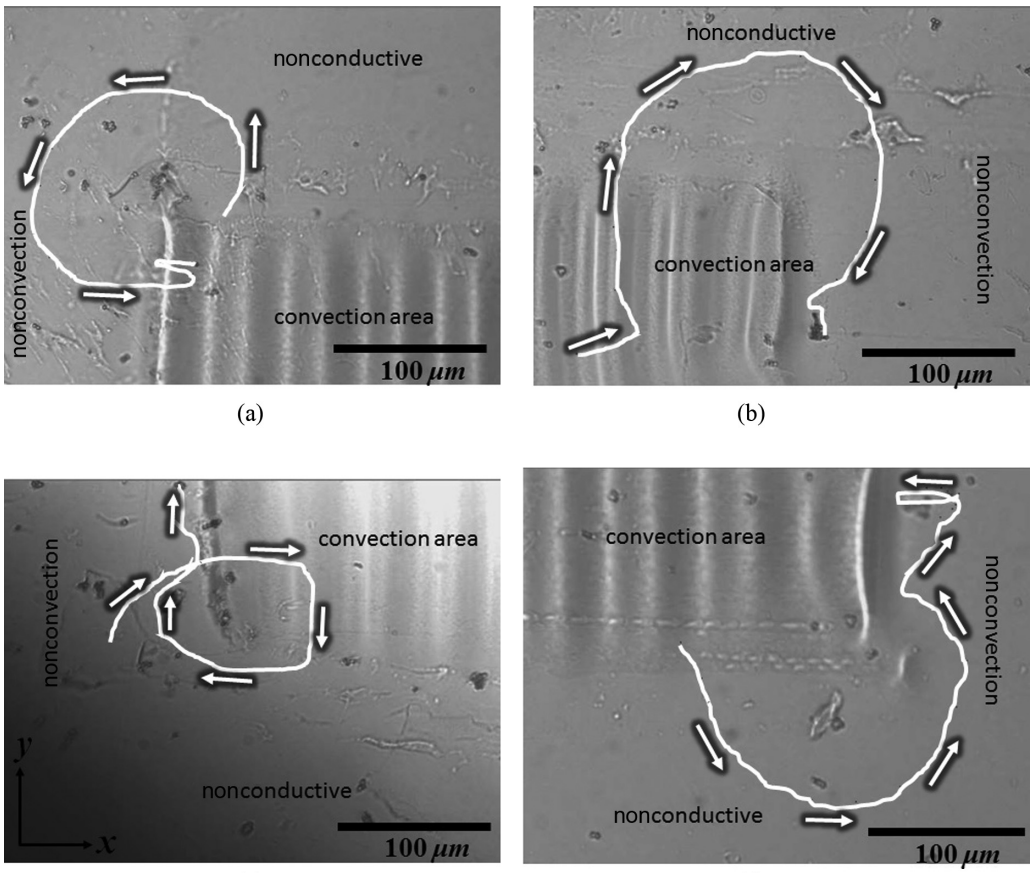

FIG. 4. Microparticle motion that indicated backflow on the (a) top-left edge, (b) top-right edge, (c) bottom-left edge, and (d) bottom-right edge in a parallelepiped cell with $\Delta l = 2$ mm, $f = 100$ Hz, and $\varepsilon = 0.05$.

is dominated by translational flow that contrasts with the convection flow. Similar results were also observed in the sample $\Delta l = 1$ mm. Furthermore, observations in the nonconvection area did not show any translational flow. This is characterized by the absence of moving microparticles in the area.

Figure 3(a) shows three kinds of particle trajectories. Path (1) shows particle movement that initially oscillates in a certain roll, crosses another roll, and then continues its oscillating motion. A similar motion is also observed for other particles in the opposite direction. The details of path (1) are shown in Fig. 3(b). Path (2) is the path of the particle moving in opposite directions along the line on the y axis. Path (2) shows the microparticle moving out of the convection area, which then shows backflow motion, as described in more detail in Figs. 4(a)–4(d). Path (3) shows the oscillating particles, indicating convective flow. Two adjacent particles appear to have opposite directions of oscillation. The three observed paths are a different mechanism than the observations in [33]. The flow in [33] is related to another pattern formation phenomenon in the high-frequency regime called "prewavy." In [33] path (1) shows a zigzag movement. However, in translational flow, this is not the case. Path (1) in translational flow shows the convection rolls driven by an electric field parallel to the director due to the accumulation of ions in the nonconvection part of the cell. Path (2) in [33] is referred to as long circular flow, while in translational flow it is related to backflow. This means that after the translational flow reaches the center of the cell, it will be pushed out of the convection area, and then move back from the edge of the cell like its initial motion.

The following discussion focuses on path (1), which is represented in the form of a graph in Fig. 3(b). Figure 3(b) depicts the motion of the microparticle (black solid line) between the first roll (black dotted line), the second roll (black dashed line), and the third roll (black dash-dotted line). The microparticle was observed every 120 s on samples $\Delta l = 1$ mm and $\varepsilon = 0.05$. The shift of the first, second, and third roll in Fig. 3(b) shows the existence of a translational flow. The rolls have shifted because of the nonconvective parts of the parallelepiped cells. Figure 3(b) also describes that, in the beginning, the microparticle oscillates between the first and second rolls from $t = 0$ to $t = 2040$ s. This oscillatory motion shows the vortex motion of liquid crystal molecules due to the application of an electric field. This solid black line also shows that as the microparticle oscillates, its diameter of trajectory will decrease over time. At $t = 2040$ s, the microparticle moves to a position between the second and third rolls. This is represented by the position of the solid black line that extends past the black dashed line. The microparticle appeared to move its position while still oscillating. This is represented by the solid black line between the black dashed and black dash-dotted lines. This result indicates that translational flow was also accompanied by the mass flow of liquid crystals.

We also investigated backflow on the phenomenon of translational flow. The motion of the microparticle was observed in four parts of the sample point, namely, at the top-left edge, bottom-left edge, top-right edge, and bottom-right edge. Figures 4(a)–4(d) represent the results. The white line and white arrows in Fig. 4 show the microparticle motion trajectory for 3600 s. Figure 4(a) shows the motion of a microparticle at the top-left edge of the parallelepiped cell. The microparticle initially moves upward, forms a circular path counterclockwise, and then returns to small oscillations. The microparticle motion on the top-right edge of the cell is shown in Fig. 4(b). Initially, a particle moves up, forms a circular path in a clockwise direction, and then returns to small oscillations. Figure 4(c) shows a microparticle motion on the bottom-left edge of the cell. First, the microparticle forms a circular path in a clockwise direction and then continues its upward motion with tiny oscillations. The microparticle motion on the bottom-right edge of the cell is shown in Fig. 4(d). Initially, the microparticle moves downward in a circular path counterclockwise and finally continues its upward motion. The calculation results show that the backflow velocity in Figs. 4(a)–4(d) is 163×10^{-3}, 110×10^{-3}, 134×10^{-3}, and 141×10^{-3} μm/s, respectively. This is in the same order as the pattern velocity in the $X = 7$ segment. This could be due to the uniform backflow velocity at the edge of the cell, as mentioned above. From all these results, we propose a translational flow scheme in Fig. 5, which shows three kinds of flow in a parallelepiped cell. These are translational flow, backflow, and convection flow.

In conclusion, by observing the motion of the microparticle, we were able to identify the flows in the parallelepiped cells. Microparticle motion is influenced by the presence of translational flow, backflow, and convection flow. The microparticle trajectories show that translational flow was also accompanied by the mass flow of liquid crystals. At the same time, the small oscillations below the threshold voltage indicate that convection flow occurs earlier than translational flow. The backflow observed at each edge of the cell indicates that flow originates from the left and right edges of the cell and moves toward the center of the cell.

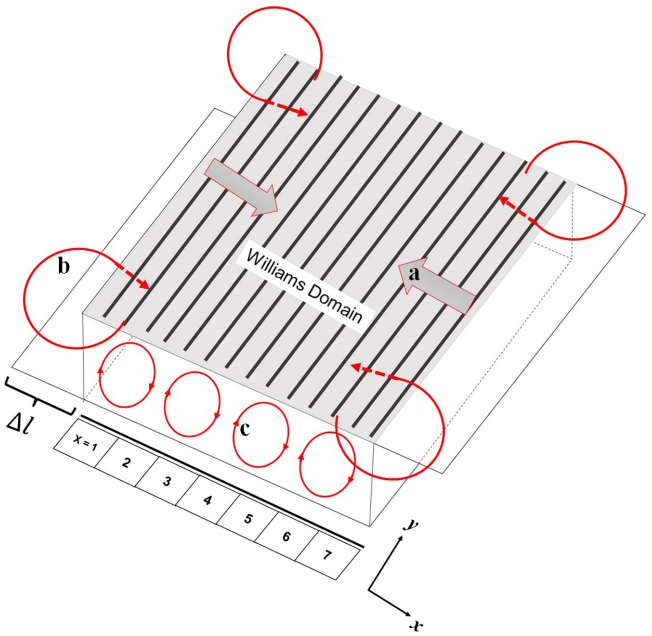

FIG. 5. Illustration of flows in a parallelepiped cell: (a) translational flow, (b) backflow, (c) convection flow.

ACKNOWLEDGMENTS

The authors gratefully acknowledge the Indonesian Ministry of Education, Culture, Research, and Technology and the Indonesian Endowment Fund for Education (LPDP KET-3689/LPDP.4/2020).

[1] R. William, J. Chem. Phys. **39**, 384 (1963).
[2] G. H. Heilmeier, J. Chem. Phys. **44**, 644 (1966).
[3] R. B. Beyer, Phys. Rev. Lett. **22**, 918 (1969).
[4] E. F. Carr, Mol. Cryst. **7**, 253 (1969).
[5] W. Helfrich, J. Chem. Phys. **51**, 4092 (1969).
[6] J. Nakauchi, M. Yokoyama, H. Sawa, and K. Okamoto, Bull. Chem. Soc. Jpn. **46**, 3321 (1973).
[7] L. Kramer and W. Pesch, Annu. Rev. Fluid Mech. **27**, 515 (1995).
[8] I. Rehberg, B. L. Winkler, M. de la Torre Juarez, S. Rasenat, and W. Schöpf, Adv. Solid State Phys. **29**, 35 (1989).
[9] E. Bodenschatz, W. Zimmerman, and L. Kramer, J. Phys. (Paris) **49**, 1875 (1988).
[10] Á. Buka and L. Kramer, *Pattern Formation in Liquid Crystal* (Springer, New York, 1996).
[11] B. Mahendra, F. Nugroho, and Y. Yusuf, Jpn. J. Appl. Phys. **57**, 021701 (2018).
[12] Á. Buka, N. Éber, W. Pesch, and L. Kramer, Phys. Rep. **448**, 115 (2007).
[13] L. M. Blinov, *Electro-Optical and Magneto-Optical Properties of Liquid Crystals* (The Universities Press, Belfast, 1983).
[14] L. M. Blinov, Sci. Prog. **70**, 263 (1986).
[15] K. Hirakawa and S. Kai, Mol. Cryst. Liq. Cryst. **40**, 261 (1977).
[16] A. Horikawa and J-H. Huh, J. Phys. Soc. Jpn. **88**, 034602 (2019).
[17] S. Kai and K. Hirakawa, Prog. Theor. Phys. **Suppl. 64**, 212 (1978).
[18] V. Steinberg, J. Fineberg, E. Moses, and I. Rehberg, Phys. D (Amsterdam) **37**, 359 (1989).
[19] S.-Q. Zhou, N. Éber, Á. Buka, W. Pesch, and G. Ahlers, Phys. Rev. E **74**, 046211 (2006).
[20] M. Treiber and L. Kramer, Mol. Cryst. Liq. Cryst. **261**, 311 (1995).
[21] M. Dennin, M. Treiber, L. Kramer, G. Ahlers, and D. S. Cannell, Phys. Rev. Lett. **76**, 319 (1996).
[22] M. Treiber, N. Éber, Á. Buka, and L. Kramer, J. Phys. II **7**, 649 (1997).
[23] M. Treiber and L. Kramer, Phys. Rev. E **58**, 1973 (1998).
[24] R. Chang and J. M. Richardson, Mol. Cryst. Liq. Cryst. **28**, 189 (1974).
[25] R. J. Turnbull, J. Phys. D **6**, 1745 (1973).

[26] B. Mahendra, F. Nugroho, and Y. Yusuf, Jpn. J. Appl. Phys. **58**, 128005 (2019).
[27] Orsay Liquid Crystal Group, Mol. Cryst. Liq. Cryst. **12**, 251 (1971).
[28] N. Oikawa, Y. Hidaka, and S. Kai, Phys. Rev. E **70**, 066204 (2004).
[29] T. Narumi, Y. Mikami, T. Nagaya, H. Okabe, K. Hara, and Y. Hidaka, Phys. Rev. E **94**, 042701 (2016).
[30] P. A. Penz, Phys. Rev. Lett. **24**, 1405 (1970).
[31] M. Bertolotti, S. Lagomarsino, F. Scudieri, and D. Sette, J. Phys. C **6**, L177 (1973).
[32] S. Kai, N. Yoshitsune, and K. Hirakawa, J. Phys. Soc. Jpn. **40**, 267 (1976).
[33] J-H. Huh, Y. Yusuf, Y. Hidaka, and S. Kai, Phys. Rev. E. **66**, 031705 (2002).
[34] Y. Mieda and K. Furutani, in *Proceedings of IEEE International Symposium on MicroNanoMechanical and Human Science* (IEEE, New York, 2006), pp. 1–6.